Handset Frame Blockage Reduction of 5G mm-Wave Phased Arrays Using Hard Surface Inspired Structure

Rodriguez Cano, Rocio; Zhao, Kun; Zhang, Shuai; Pedersen, Gert Frølund

Published in:
I E E E Transactions on Vehicular Technology

DOI (link to publication from Publisher):
10.1109/TVT.2020.2996360

Publication date:
2020

Document Version
Accepted author manuscript, peer reviewed version

Handset Frame Blockage Reduction of 5G mm-Wave Phased Arrays Using Hard Surface Inspired Structure

Rocio Rodriguez-Cano, *Student Member, IEEE*, Kun Zhao, Shuai Zhang, *Senior Member, IEEE* and Gert Frølund Pedersen, *Member, IEEE*

***Abstract*—In this paper, the propagating characteristics of hard surfaces are employed to reduce the main beam blockage of the handset frame to horizontally polarized endfire millimeter-wave (mm-wave) arrays. To prove the concept, a quad-element vivaldi array is located at the top part of the handset and the frame with grooves is placed in front of it. The groove dimensions that form the hard surface inspired structure are studied to provide the best gain and reflection coefficient performance. The impedance bandwidth achieved is 25.3-27.5 GHz. The radiation pattern plots show that the main beam direction corresponds to endfire, the same as the original array without the frame. The mm-wave array provides beam-steering properties with a scanning angle of $\pm 65^{\circ}$ for a realized gain higher than 7 dBi.**

***Index Terms*—5G mobile communication, antenna array, cellular phones, radiation pattern.**

I. Introduction

The upcoming fifth generation of mobile communication (5G) includes new frequency bands in the millimeter-wave (mm-wave) range to cope with the saturation of the spectrum below 7 GHz [1]–[3]. The new frequency bands have motivated the appearance of many mm-wave antenna array designs for mobile phones. To compensate for the higher propagation losses and highly randomness in the wireless channel, antenna systems are required to have high gain and large beam-steering angle. Many of the designs in literature correspond to planar endfire arrays [4]–[13]. However, most of the solutions do not take into account the phone bezel. The placement of the handset metallic bezel in front of endfire mm-wave antennas can be detrimental to their radiation pattern, causing the partial or full obstruction of the main beam. Therefore, reducing the obstruction of metallic phone bezels is a critical step to implement endfire arrays in mobile handsets successfully. In previous studies from the authors, it was shown that the radiation pattern blockage is significant in the case of horizontal polarization, whilst the radiation pattern of antennas with vertical polarization remains almost unaffected [14]. For that reason, this paper only focuses on the horizontal polarization. There are some papers that consider the effect of the frame in the embedding of mm-wave arrays. In [14], two parasitic layers are added at both sides of the frame to redirect the radiation pattern to the endfire direction as a result of the energy coupling from the frame. The proposed solution in [15] consists of etching a window in the frame to place the mm-wave module. The design presented in [16] etches several vertical slots on the center of the frame to function as a second array and enhance the main beam gain. In this paper, the concept of hard surfaces is employed to reduce the frame blockage to mm-wave antennas by decreasing the edges diffraction.

The term hard surface comes from acoustics. In electromagnetism, it is used to designate an ideal conductor that is corrugated with longitudinal grooves that are filled with dielectric material [17]. This type of structure supports the wave propagation through it, with a maximum value of the E-field at the surface. If the surface is loaded with dielectric material in the z direction (according to the coordinate system in Fig. 1), with the proper design, the corrugated structure can behave as a hard surface for both vertical and horizontal polarizations. This concept has been employed in literature to reduce the forward scattering in the case of cylindrical struts in antennas with parabolic reflectors. In [18], the struts and masts are constructed using hard surfaces, reducing the sidelobes caused by the inherent blockage.

To illustrate the concept, Fig. 1 (a) shows a mm-wave vivaldi array with a 10 mm-thick frame in front of it. The frame is a piece of metal with overall dimensions 5 mm $\times$88 mm $\times$10 mm, and it is placed 1 mm away from the top part of the mm-wave array. The vivaldi array has horizontal polarization, i.e. x axis direction, and has end-fire radiation [14]. The side view of the electric field is represented in Fig. 1 (c). As can be seen, the E-field is diffracted by the frame and the main beam direction changes from endfire to other directions. For that reason, mm-wave arrays for the upcoming 5th generation of mobile communication need to consider the effect of the frame in the antenna design. When the frame is incorporated, the electric field is diffracted backward and the radiation pattern becomes broadside (Fig. 1 (e)). The principle of operation consists in supporting the wave propagation through the frame (in the z axis direction) to reduce its blockage width. Since the wave is allowed to propagate through the frame when the hard surface inspired design is employed (Fig. 1 (b)), less energy is diffracted and the main beam points to the original direction (Fig. 1 (f)). To provide a hard surface behaviour, two

This work was supported by the InnovationsFonden project of Reconfigurable Arrays for Next Generation Efficiency (RANGE).

Rocio Rodriguez-Cano, Kun Zhao, Shuai Zhang and Gert F. Pedersen are with the Antenna, Propagation and Millimeter-Wave Section (APMS) at the Department of Electronic Systems, Aalborg University, 9220 Aalborg, Denmark. Corresponding author Shuai Zhang (e-mail: sz@es.aau.dk).

Kun Zhao is also with Sony Research Center Lund, Sweden.

Manuscript received XXX, XX, 2020; revised XXX, XX, 2020.

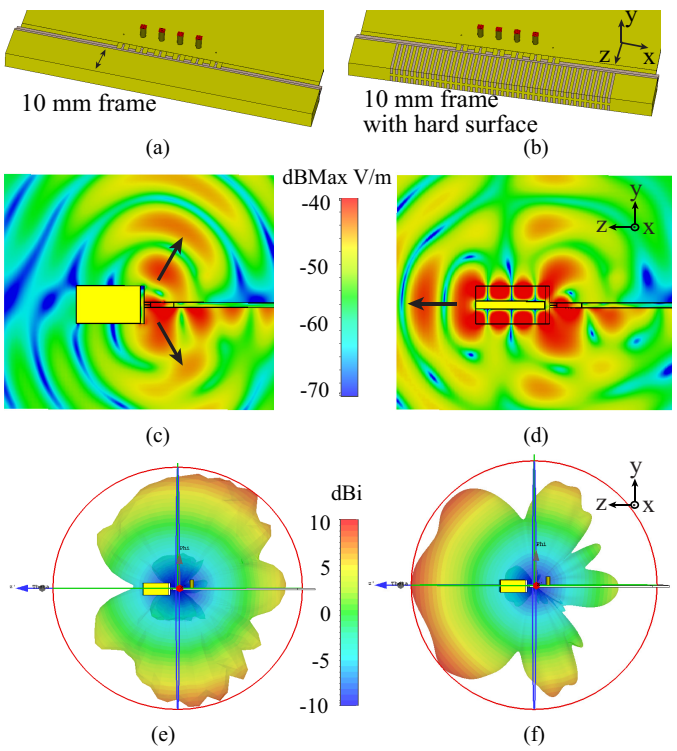

Fig. 1. (a) Front view of the mm-wave array with a 10 mm-thickness frame. (b) Front view of mm-wave array with a hard surface. (c) YZ plane cut of the E-field of (a). (d) YZ plane cut of the E-field of (b). (e) Realized gain radiation pattern of the $\Phi = 90^\circ$ cut of (a). (f) $\Phi = 90^\circ$ cut of (b).

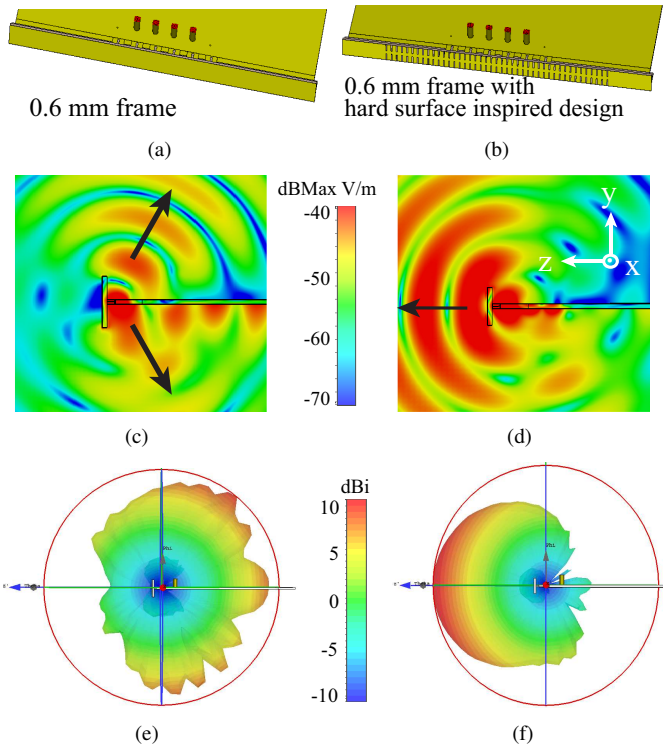

Fig. 2. (a) Front view of the mm-wave array with a 0.6 mm-thickness frame. (b) Front view of mm-wave array with a hard surface inspired frame. (c) YZ plane cut of the E-field of (a). (d) YZ plane cut of the E-field of (b). (e) Realized gain radiation pattern of the $\Phi = 90^\circ$ cut of (a). (f) $\Phi = 90^\circ$ cut of (b).

rows of grooves have been etched on the frame and then filled with dielectric material. This solution does not require any large windows or extra structures. The proposed mechanism is demonstrated with a manufactured prototype of the frame with two rows of grooves in front of a vivaldi array. Measurements and simulations show good agreement. Simulations are carried out by CST Microwave Studio 2019.

II. Metal Frame with Corrugated Edges

The phone bezel is significantly thinner than 10 mm, which was the example width employed in the introduction. The same hard surface concept can be extended to commercial models to make the main beam radiate in the original direction, as shown in Fig. 2. It can be considered as cutting a thin slice of the previous 10 mm-thick frame, as detailed in Fig. 3. The frame is formed by a substrate of $\epsilon_r = 6$ with a metallic layer on the outer side, and it is placed 1 mm away from the mm-wave array.

In order to demonstrate the effect from the corrugated edges on reducing the blockage of the metal frame, a horizontally polarized plane wave illuminates the metal frame from a normal angle of incidence, as shown in Fig. 4. There is no air space between the frame and the open boundary condition on $+x$ and $-x$ direction to exclude the scattering on the short edge of the frame. The corresponding electrical field at 22 GHz is represented in Fig. 5 (a), where the groove length is $l_{hs} = 2$ mm. To show the effect of the corrugated hard surface inspired design, two reference frame structures without grooves are also

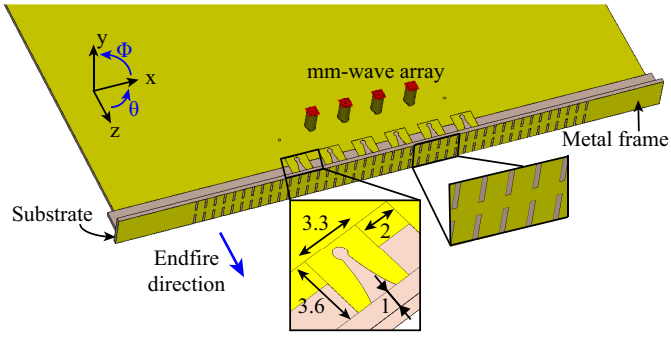

Fig. 3. Geometry of the proposed antenna.

shown, one 1 mm wide and the other 5 mm wide. The plane wave propagation in free space has also been given. It can be observed that the E-field is guided over the metal frame through the corrugated edge, and the blockage on the E-field is considerably reduced.

To further quantify the effect from the corrugated structure, the corresponding monostatic radar cross section (RCS) has also been calculated. The monostatic RCS measures the power scattered back by the metal frame, and therefore, it is preferred to have a small RCS for the metal frame to reduce the blockage effect. In Fig. 6, the RCS of the different cases discussed has been plotted. A clear reduction in the RCS value can be observed by using the corrugated metal frame ($l_{hs} = 2$ mm), and the RCS of the metal frame can be reduced a wide band comparing to the 1 mm-wide frame. On the other hand, the

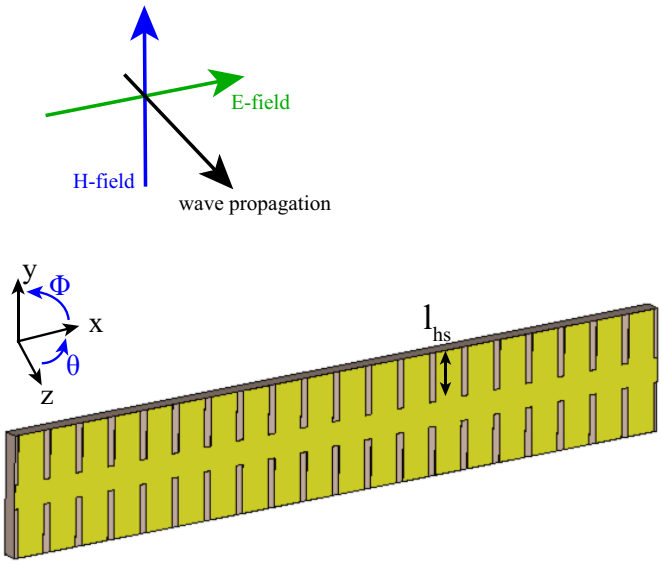

Fig. 4. Plane wave illuminating a 30 mm-long frame. The polarization of the plane wave is marked with arrows (the electric field corresponds to the green arrow).

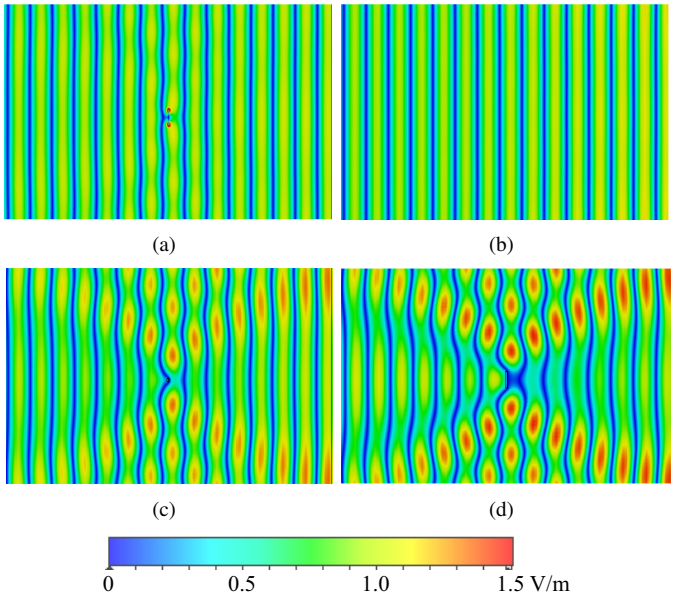

Fig. 5. E-field at 22 GHz in the YZ plane. (a) With corrugations. (b) Free space. (c) With a 1 mm-width frame. (d) With a 5 mm-width frame.

operating band of the corrugated frame can be controlled by tuning the length of the slot (l_{hs}), which can make the design be fitted in different bands of interest in a practical phone design. The corrugation of the final design has a length of $l_{hs} = 2$ mm. The lengths employed for the shorter and longer corrugations are 1.75 mm and 2.25 mm, respectively.

It is worth mentioning that the above analysis is based on a plane wave with normal angle of incidence. In practice, the mm-wave antennas for mobile phones will be placed very close to the phone bezel and thus, the plane wave assumption used above will not be valid. In order to verify that the proposed design can operate properly in a practical design, the analysis based on a device with smartphone form factor

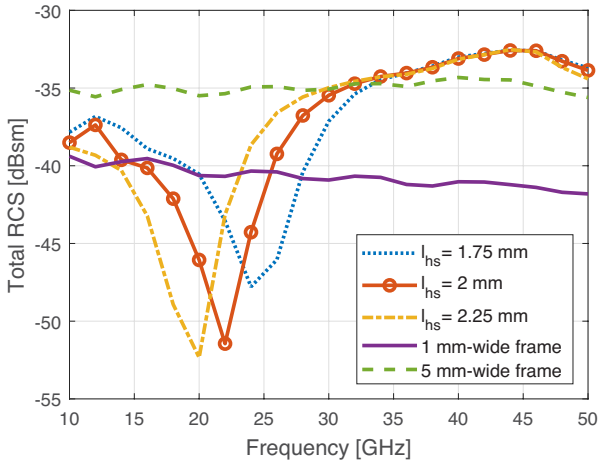

Fig. 6. Radar cross section (RCS) of different frame configurations.

will be given in the next section. In fact, in the next section the operating frequency is shifted up with the full phone model and the same groove length.

III. Proposed Mechanism

In order to demonstrate that the structure performs like a hard surface and it is not due to the partial reduction of the frame width because of the grooves, four different configurations are further compared in Fig. 7. The in-phase combination of all the array elements is plotted as a function of the frequency. IEEE gain is chosen as it does not consider the mismatching losses, that can be different according to the frame width. The gain curve of the vivaldi array without frame has been added as a reference. The following two configurations correspond to the frame without grooves of width 1 and 5 mm, respectively. The last curve represents a 5 mm-width frame with the grooves forming the hard surface inspired design. The space between the two groove rows is 1 mm. As it can be seen, the frame with corrugations is 2 dBi higher than the 1 mm-width frame and almost 10 dBi higher than the 5 mm-width metal frame. The gain improves 1 dB with respect to the array with no frame at 25 GHz.

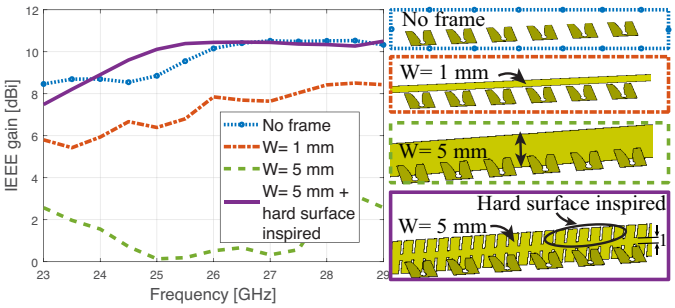

Fig. 7. Combined endfire IEEE gain (in the $+z$ axis direction) frequency evolution according to frame width.

Mm-wave phased arrays are supposed to scan the beam in different directions and achieve high gain. The simulated

beam-steering envelope of the mm-wave array with the frame with grooves is represented in Fig. 8. The envelope is formed by the maximum gain of 12 beams, with a phase difference of 30°. The beam is able to scan ±65° with a gain higher than 7 dBi. With 7 dBi array gain, the 5G mm-wave UE can meet the 3GPP EIRP requirement [19], with a limited TRP level in the band of interest. Therefore, we define here the scanning angles according to 7 dBi. The gain in the boresight direction reaches 10 dBi, while when the phase difference between the elements is 150°, the gain is around 7 dBi. That is due to the vivaldi element radiation pattern. In Fig. 8(b) the realized gain envelope is represented for different frequencies. The gain drop at 25 GHz is due to the fact that the impedance matching is degraded and the realized gain takes into account the mismatching losses.

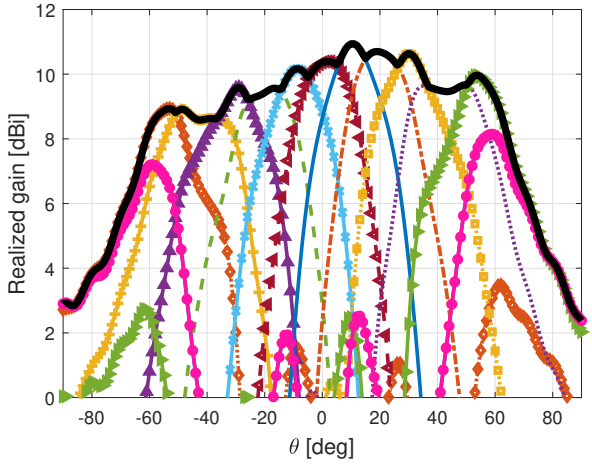

(a)

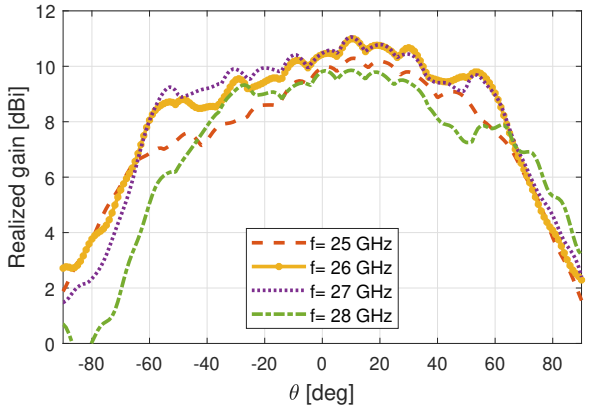

(b)

Fig. 8. $\Phi = 0°$ cut of: (a) simulated realized gain beam scanning from -65° to 65° and beam-steering envelope at 26 GHz. (b) Simulated realized gain beam-steering envelope at different frequencies.

IV. Parametric Studies

The operating frequency, groove dimensions, and other design factors can be controlled to meet the demand of various phone form factors. This section comprises the most important parameters in the design of the hard surfaces. The assessed parameters are: groove length, the effect of the substrate dielectric constant, groove periodicity and groove width.

A. Groove length

The length of the grooves etched on the frame has a strong influence on the gain of the array and the reflection coefficient, as shown in Fig. 9. For this study, a dielectric permittivity of 6 is chosen. For a length $l_{hs} = 0$ mm, i.e. full 5 mm-width frame without any grooves, the gain in the endfire direction ($+z$ axis) between 24 and 28 GHz is below to 2 dBi. Increasing the length of the groove reduces the frame blockage and allows the electric field to propagate through and for that reason, the gain increases. A value of 2 mm has been chosen to maximize the impedance bandwidth and obtain high gain. If this value is expressed in wavelength terms, $\lambda_g/4 < l_{hs} < \lambda_g/2$.

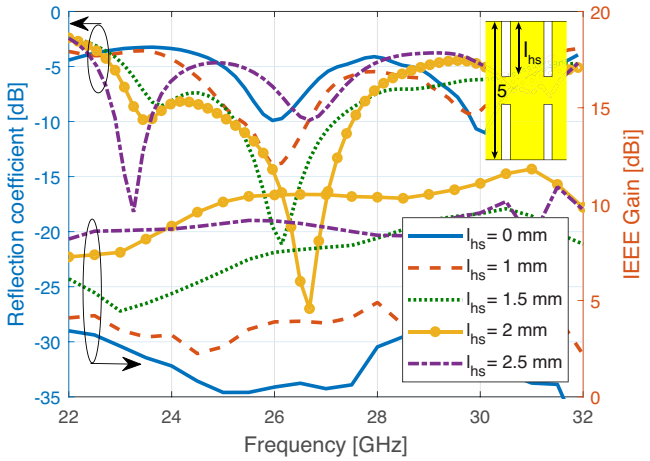

Fig. 9. Reflection coefficient and IEEE gain in the endfire direction for different lengths of the grooves.

B. Effect of the dielectric constant

The dielectric constant of the frame substrate is another parameter to consider. Fig. 10 shows how an increase in the permittivity provides higher gain. The value of ϵ_r that presents a broad impedance bandwidth with high gain is 6. A gain increment is observed in Fig. 10 when the permittivity of the substrate is increased. However, this gain increment only occurs when the frame is composed of dielectric and the modified metal. When only dielectric is placed in front of the array, an increase in the substrate permittivity does not translate into an increase of gain, but a shift of the curve towards lower frequencies. As mentioned in the previous subsection, the groove length can be expressed in wavelength terms. The guided wavelength (λ_g) is defined as the free-space wavelength divided by the square root of the dielectric constant. It is important to consider that these results are obtained without tuning the mm-wave array or the groove dimensions. If there is the possibility of modifying and matching the array, a frame substrate with a higher dielectric constant can be chosen, resulting in grooves with a shorter length. This could make the hard surface solution less noticeable to the frame design

and increase the mechanical robustness. The results for an optimized $\epsilon_r = 10$ have also been included in Fig. 10. Only the groove length has been modified to $l_{hs} = 1.5$ mm. The impedance bandwidth is smaller than the one obtained with the chosen permittivity, but the gain increases 0.8 dBi. It can also be observed that the gain performance in the band of interest is similar with the optimized designs for different substrate permittivities, which also verifies that the gain enhancement is not related to the increment in the permittivity.

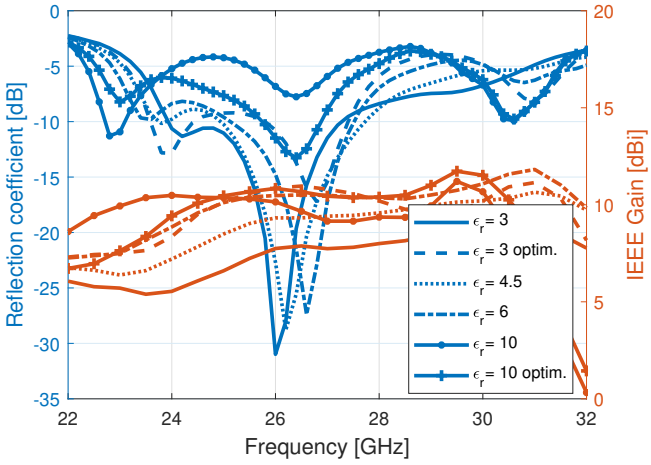

Fig. 10. Reflection coefficient and IEEE gain in the endfire direction for different dielectric constants.

C. Groove periodicity

The groove periodicity is another critical parameter and it is represented in Fig. 11. Broader separations provide in general higher gain, but narrower impedance bandwidth. A periodicity of 1.5 mm is chosen for the design not to limit considerably the impedance bandwidth. The periodicity has to be smaller than $\lambda/2$.

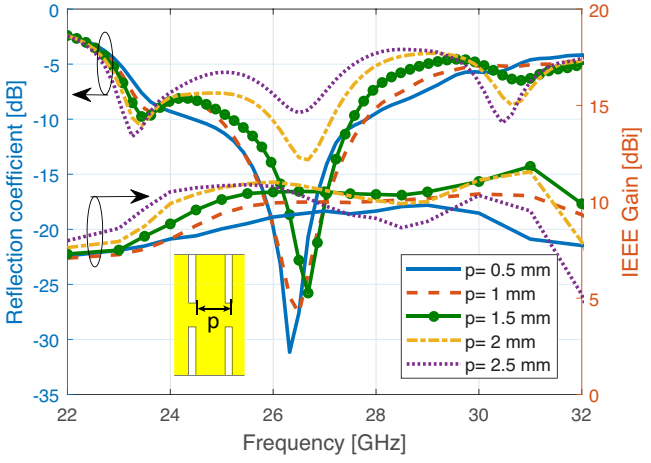

Fig. 11. Reflection coefficient and IEEE gain in the endfire direction for different periodicity.

D. Groove width

The effect of the grooves width is represented in Fig. 12. The width is not as critical as the length, but there is a trade-off between gain and impedance bandwidth. For a fixed periodicity of the grooves etched, the narrower the groove is, the wider the strip would be. Therefore, the gain is higher at lower frequencies. The impedance bandwidth is, however, narrower when the width of the groove is reduced. Due to this compromise, a width of $W_{hs} = 0.3$ mm is chosen for the design.

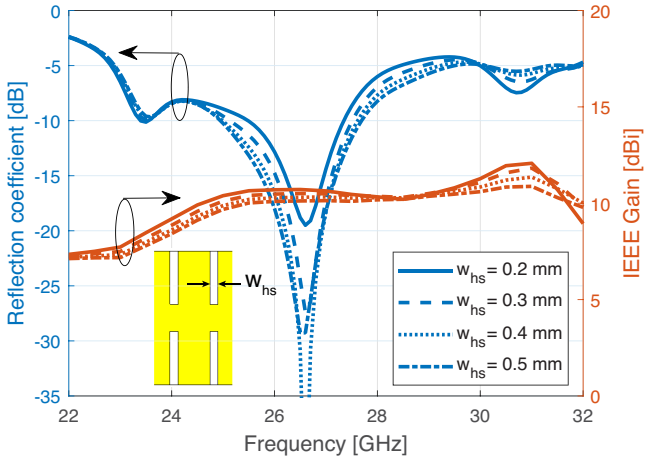

Fig. 12. Reflection coefficient and IEEE gain in the endfire direction for different widths of the grooves.

To sum up, the groove length is the most critical parameter. In addition, the dielectric permittivity of the frame substrate and periodicity of the grooves have also a strong influence on the gain and impedance curves. By properly tuning these parameters, the proposed method can be implemented for different operating frequencies and phone form factors.

V. Final Design and Results

The parametric studies from Section IV have provided the optimum design parameters for the frame inspired in hard surfaces. The final design corresponds with the model of Fig. 3, and the final parameter values are listed in Table I. The parameter w_{frame}, corresponds to the frame width and t_{subs} is the thickness of the frame substrate. The mm-wave array is located at the top part of the PCB and is formed by 4 active vivaldi elements and 2 grounded elements at the opposite ends to provide similar boundary conditions. The metallic frame with grooves is placed 1 mm away from the array. The frame is also made of the same kind of PCB of $\epsilon_r = 6$, and only one metalized side. A prototype has been fabricated and it is represented in Fig. 13. As mentioned in Section IV, the aim of this publication is to design the frame to reduce the blockage. The mm-wave vivaldi array used to prove the principle is carried out in [14]. Throughout this section, the performance of the prototype is evaluated.

The scattering parameters are plotted in Fig. 14. The antenna is matched below -10 dB from 23.6 to 27.5 GHz. The coupling between the central elements of the array is lower than -15

TABLE I
FINAL DESIGN PARAMETERS

l_{hs}	w_{hs}	p	$Ant.\text{-}frame$ $distance$	w_{frame}	ϵ_r	t_{subs}
2 mm	0.3 mm	1.5 mm	1 mm	5 mm	6	0.635 mm

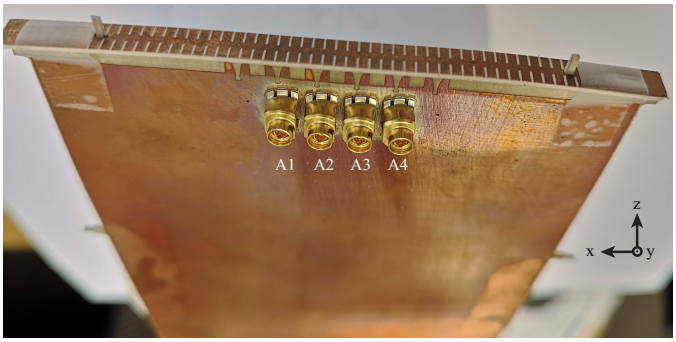

Fig. 13. Fabricated prototype. Only the top part of the PCB is shown.

dB in all the impedance bandwidth. The total efficiency of the array is higher than 90 % in the operating bandwidth, reaching a maximum value of 94 % at 26.5 GHz.

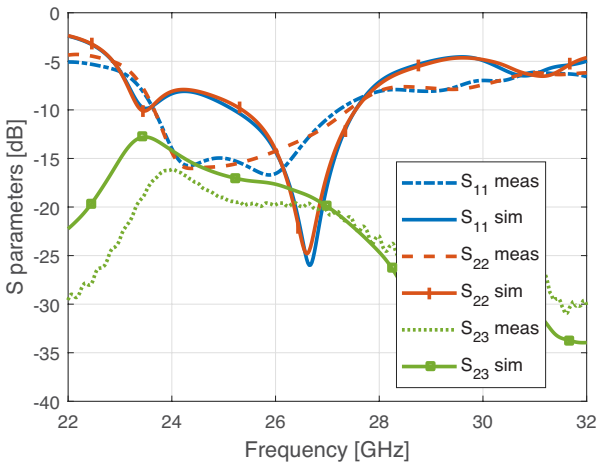

Fig. 14. S parameters comparison between measurements and simulations.

Fig. 15 shows the measurement set-up for the radiation pattern measurements. Due to the absorber placed behind the antenna, the angle θ is only displayed until 150°. The measurement procedure is described next. The phase center of the measurement system is located first. Afterwards, the center of the array is placed at the phase center of the measurement system. Each antenna element is measured without changing the position of the array. The combined gain can be computed as the sum over all the elements of the measured gain pattern of the antenna element multiplied by the phase shift at the feed of the element.

The combined radiation pattern of all the elements in phase is depicted in Fig. 16 for the $\Phi = 0°$ and $\Phi = 90°$ cuts. The main beam points to the endfire direction and the sidelobe level is -11.9 dB (Fig. 16 (a)). The fact that the array is broad

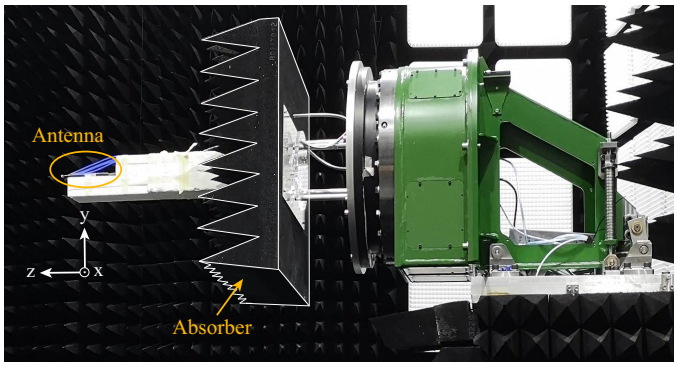

Fig. 15. Measurements set-up of the chamber.

in θ is favourable to achieve a 360° beam-steering coverage. A maximum realized gain of 10.2 dBi is obtained in the endfire direction. The combined radiation pattern has also been plotted in Fig. 17 for different phase shifts among the elements ($\Delta\phi = 0°, 90°, 150°$) and for different frequencies. Good agreement is found between measurements and simulations. The evolution of the endfire realized gain as a function of the frequency is shown in Fig. 18. The combined gain is higher than 7 dBi in all the operating band of 25.3-27.5 GHz, with a value of approximately 10 dBi from 25-26.5 GHz. Similar gain behaviour is found between the symmetric elements both in the measurements and simulations. Due to the detuning of the antenna, the gain is lower at the higher frequencies.

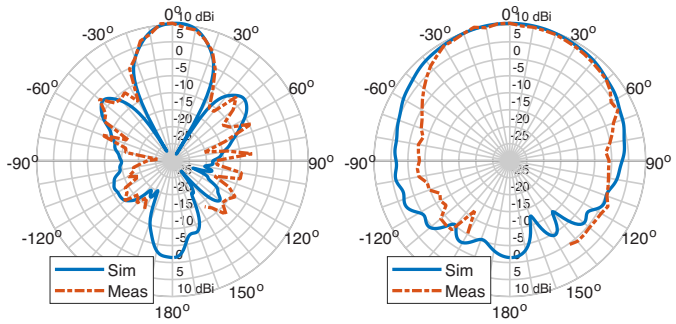

(a) (b)

Fig. 16. Combined realized gain in-phase radiation pattern at 26 GHz. (a) $\Phi = 0°$ cut. (b) $\Phi = 90°$ cut.

VI. CONCLUSION

This paper presents a new method to decrease the blockage of metal frames to endfire mm-wave arrays with horizontal polarization by using a hard surface inspired design on the frame. The grooves can reduce the diffraction on the edges. The electric field is permitted to propagate through the frame and the energy diffracted is significantly reduced. A vivaldi mm-wave array has been used to test the performance and the results show good agreement with the simulations. The beam-steering scanning range is ±65° with a gain higher than 7 dBi.

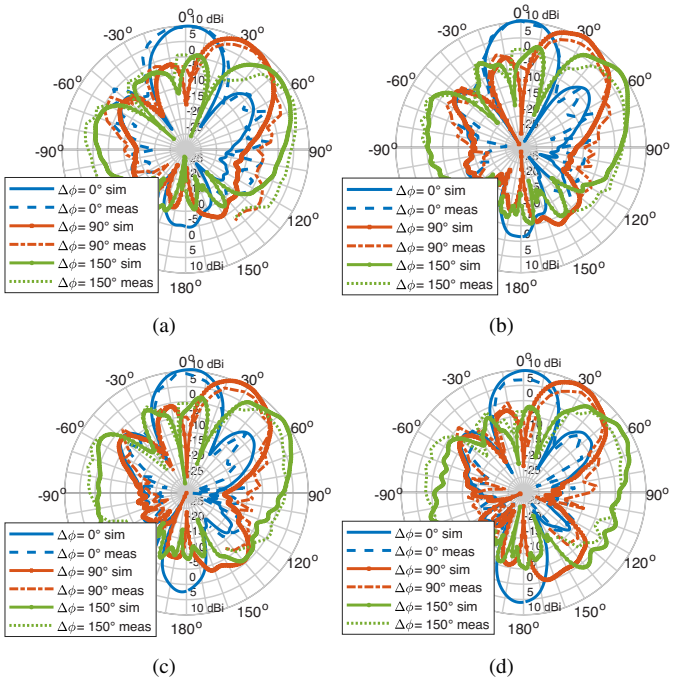

Fig. 17. Combined realized gain radiation pattern for different phase shifts ($\Delta\phi = 0°, 90°, 150°$) in the $\Phi = 0°$ cut. (a) 25 GHz. (b) 26 GHz. (c) 27 GHz. (d) 28 GHz.

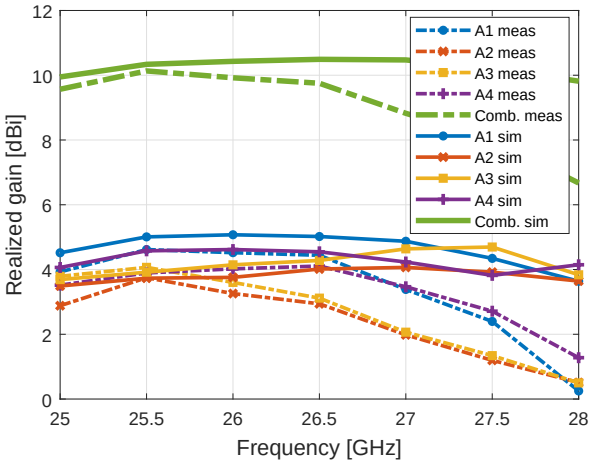

Fig. 18. Endfire realized gain of each antenna as a function of the frequency. The combined in-phase gain is also represented.

ACKNOWLEDGMENT

The authors would like to thank Ben Krøyer and Kim Olesen for their help with the manufacturing and measurement, respectively.

REFERENCES

[1] S. Sun, T. S. Rappaport, M. Shafi, P. Tang, J. Zhang, and P. J. Smith, "Propagation models and performance evaluation for 5g millimeter-wave bands," *IEEE Trans. Veh. Technol.*, vol. 67, no. 9, pp. 8422–8439, Sep. 2018.

[2] J. Lota, S. Sun, T. S. Rappaport, and A. Demosthenous, "5g uniform linear arrays with beamforming and spatial multiplexing at 28, 37, 64, and 71 ghz for outdoor urban communication: A two-level approach," *IEEE Transactions on Vehicular Technology*, vol. 66, no. 11, pp. 9972–9985, Nov 2017.

[3] S. Zhang, X. Chen, and G. F. Pedersen, "Mutual coupling suppression with decoupling ground for massive mimo antenna arrays," *IEEE Transactions on Vehicular Technology*, vol. 68, no. 8, pp. 7273–7282, Aug 2019.

[4] I. Hwang, B. Ahn, S. Chae, J. Yu, and W. Lee, "Quasi-yagi antenna array with modified folded dipole driver for mmwave 5g cellular devices," *IEEE Antennas Wireless Propag. Lett.*, vol. 18, no. 5, pp. 971–975, May 2019.

[5] M. M. Samadi Taheri, A. Abdipour, S. Zhang, and G. F. Pedersen, "Integrated millimeter-wave wideband end-fire 5g beam steerable array and low-frequency 4g lte antenna in mobile terminals," *IEEE Trans. Veh. Technol.*, vol. 68, no. 4, pp. 4042–4046, April 2019.

[6] H. Ozpinar, S. Aksimsek, and N. Turker Tokan, "A novel compact, broadband, high gain millimeter-wave antenna for 5g beam steering applications," *Accepted in IEEE Trans. Veh. Technol.*, 2019.

[7] C. Di Paola, S. Zhang, K. Zhao, Y. Zhinong, T. Bolin, and G. F. Pedersen, "Wideband beam-switchable 28 ghz quasi-yagi array for mobile devices," *IEEE Trans. Antennas Propag.*, pp. 1–1, 2019.

[8] Y. Hsu, T. Huang, H. Lin, and Y. Lin, "Dual-polarized quasi yagi–uda antennas with endfire radiation for millimeter-wave mimo terminals," *IEEE Trans. Antennas Propag.*, vol. 65, no. 12, pp. 6282–6289, Dec 2017.

[9] J. Zhang, K. Zhao, L. Wang, S. Zhang, and G. F. Pedersen, "Dual-polarized phased array with endfire radiation for 5g handset applications," *IEEE Trans. Antennas Propag.*, pp. 1–1, 2019.

[10] R. A. Alhalabi and G. M. Rebeiz, "Differentially-fed millimeter-wave yagi-uda antennas with folded dipole feed," *IEEE Trans. Antennas Propag.*, vol. 58, no. 3, pp. 966–969, March 2010.

[11] C. Di Paola, K. Zhao, S. Zhang, and G. F. Pedersen, "Siw multibeam antenna array at 30 ghz for 5g mobile devices," *IEEE Access*, vol. 7, pp. 73 157–73 164, 2019.

[12] B. Xu, Z. Ying, L. Scialacqua, A. Scannavini, L. J. Foged, T. Bolin, K. Zhao, S. He, and M. Gustafsson, "Radiation performance analysis of 28 ghz antennas integrated in 5g mobile terminal housing," *IEEE Access*, vol. 6, pp. 48 088–48 101, 2018.

[13] Y. Luo, J. Xu, Y. Chen, Y. Sun, B. Xu, S. Xu, and G. Yang, "A zero-mode induced mmwave patch antenna with low-profile, wide-bandwidth and large-angle scanning for 5g mobile terminals," *IEEE Access*, vol. 7, pp. 177 607–177 615, 2019.

[14] R. Rodriguez-Cano, S. Zhang, K. Zhao, and G. F. Pedersen, "Reduction of main beam-blockage in an integrated 5g array with a metal-frame antenna," *IEEE Trans. Antennas Propag.*, vol. 67, no. 5, pp. 3161–3170, May 2019.

[15] J. Kurvinen, H. Kähkönen, A. Lehtovuori, J. Ala-Laurinaho, and V. Viikari, "Co-designed mm-wave and lte handset antennas," *IEEE Trans. Antennas Propag.*, vol. 67, no. 3, pp. 1545–1553, March 2019.

[16] R. Rodriguez-Cano, S. Zhang, K. Zhao, and G. F. Pedersen, "Mm-wave beam-steerable endfire array embedded in slotted metal-frame lte antenna," *Accepted in IEEE Trans. Antennas Propag.*, December 2019.

[17] P. Kildal, "Artificially soft and hard surfaces in electromagnetics," *IEEE Trans. Antennas Propag.*, vol. 38, no. 10, pp. 1537–1544, Oct 1990.

[18] P. Kildal, A. A. Kishk, and A. Tengs, "Reduction of forward scattering from cylindrical objects using hard surfaces," *IEEE Trans. Antennas Propag.*, vol. 44, no. 11, pp. 1509–1520, Nov 1996.

[19] "General aspects for User Equipment (UE) Radio Frequency (RF) for NR (Release 15)," 3rd Generation Partnership Project (3GPP), Technical Report (TR) 38.817-1, 03 2019, version 15.3.0.

Rocio Rodriguez-Cano (S'17) was born in Granada (Spain) in 1993. She received the B.S. degree and MsC. in Electrical Engineering at the University of Malaga, Spain, in 2015 and 2017, respectively. She is currently pursuing a Ph.D. in antenna systems for the next generation of mobile terminals at Aalborg University, Denmark. In November 2019, she was a Visiting Ph.D. Student with the Global Big Data Technologies Centre, University of Technology Sydney, Australia. Her current research interests include antenna design for 5G communications, integration with the former generations of mobile communications, user exposure and small antennas.

Kun Zhao received the B.S. degree in Communication Engineering from Beijing University of Posts and Telecommunications (BUPT), Beijing, China in 2010, M.S. in wireless systems and Ph.D. degree in electromagnetic engineering from Royal Institute of Technology (KTH), Stockholm, Sweden, in 2012 and 2017, respectively. Currently, he is a researcher of antenna technology and standardization in the Radio Access Lab, Sony Mobile Communication AB, Lund, Sweden. He also works as an industrial post-doc at Aalborg University, Denmark. He was a visiting researcher at the Department of Electrical and Information Technology, Lund University, Sweden. His current research interests include mm-wave antenna and propagation for 5G communications, MIMO antenna systems, user body interactions, and body centric wireless communications.

Shuai Zhang (SM'18) received the B.E. degree from the University of Electronic Science and Technology of China, Chengdu, China, in 2007 and the Ph.D. degree in electromagnetic engineering from the Royal Institute of Technology (KTH), Stockholm, Sweden, in 2013. After his Ph.D. studies, he was a Research Fellow at KTH. In April 2014, he joined Aalborg University, Denmark, where he currently works as Associate Professor. In 2010 and 2011, he was a Visiting Researcher at Lund University, Sweden and at Sony Mobile Communications AB, Sweden, respectively. He was also an external antenna specialist at Bang & Olufsen, Denmark from 2016-2017. He has coauthored over 50 articles in well-reputed international journals and over 15 (US or WO) patents. His current research interests include: mobile terminal mmwave antennas, biological effects, CubeSat antennas, Massive MIMO antenna arrays, UWB wind turbine blade deflection sensing, and RFID antennas.

Gert Frølund Pedersen (M'14) was born in 1965. He received the B.Sc. and E.E. (Hons.) degrees in electrical engineering from the College of Technology in Dublin, Dublin Institute of Technology, Dublin, Ireland, in 1991, and the M.Sc.E.E. and Ph.D. degrees from Aalborg University, Aalborg, Denmark, in 1993 and 2003, respectively. Since 1993, he has been with Aalborg University where he is a Full Professor heading the Antennas, Propagation and Millimeter-wave Systems LAB with 25 researchers. He is also the Head of the Doctoral School on wireless communication with some 40 Ph.D. students enrolled. His research interests include radio communication for mobile terminals especially small antennas, diversity systems, propagation, and biological effects. He has published more than 500 peer reviewed papers, 6 books, 12 book chapters and holds over 50 patents. He has also worked as a Consultant for developments of more than 100 antennas for mobile terminals including the first internal antenna for mobile phones in 1994 with lowest SAR, first internal triple-band antenna in 1998 with low SAR and high TRP and TIS, and lately various multiantenna systems rated as the most efficient on the market. He has worked most of the time with joint university and industry projects and have received more than 21 M$ in direct research funding. He is currently the Project Leader of the RANGE project with a total budget of over 8 M$ investigating high performance centimetre/millimetre-wave antennas for 5G mobile phones. He has been one of the pioneers in establishing over-the-air measurement systems. The measurement technique is now well established for mobile terminals with single antennas and he was chairing the various COST groups with liaison to 3GPP and CTIA for over-the-air test of MIMO terminals. He is currently involved in MIMO OTA measurement.